Am J Cancer Res 2024;14(2):709-726
www.ajcr.us /ISSN:2156-6976/ajcr0154043

Original Article

FLNB overexpression promotes tumor progression and associates with immune suppression, evasion and stemness in pancreatic cancer

Guoyong Fan[1*], Qian Yan[1,2*], Yubin Chen[1,2*], Mingqian Han[1], Zelong Wu[1], Shiye Ruan[1], Hongkai Zhuang[3#], Qing Gou[4#], Baohua Hou[5,1,2#]

[1]Department of General Surgery, Guangdong Provincial People's Hospital (Guangdong Academy of Medical Sciences), Southern Medical University, Guangzhou, Guangdong, China; [2]School of Medicine South China University of Technology, Guangzhou, Guangdong, China; [3]Sun Yat-sen University Cancer Center, Guangzhou, Guangdong, China; [4]Department of Interventional Radiology, Guangdong Provincial People's Hospital (Guangdong Academy of Medical Sciences), Southern Medical University, Guangzhou, Guangdong, China; [5]Heyuan People's Hospital, Heyuan, Guangdong, China. [*]Equal contributors. [#]Equal contributors.

Received October 22, 2023; Accepted February 11, 2024; Epub February 15, 2024; Published February 28, 2024

Abstract: Pancreatic cancer (PC) is an immunosuppressive cancer. Immune-based therapies that enhance or recruit antitumor immune cells into the tumor microenvironment (TME) remain promising strategies for PC treatment. Consequently, a deeper understanding of the molecular mechanisms involved in PC immune suppression is critical for developing immune-based therapies to improve survival rates. In this study, weighted gene co-expression network analysis (WGCNA) was used to identify Filamin B (FLNB) correlated with the infiltration of $CD8^+$ T cells and tumor-associated macrophages (TAMs). The clinical significance and potential biological function of FLNB were evaluated using bioinformatic analysis. The oncogenic role of FLNB in PC was determined using *in vitro* and *in vivo* studies. We further analyzed possible associations between FLNB expression and tumor immunity using CIBERSORT, single sample gene set enrichment analysis, and ESTIMATE algorithms. We found FLNB was overexpressed in PC tissues and was correlated with poorer overall survival, tumor recurrence, larger tumor size, and higher histologic grade. Moreover, FLNB overexpression was associated with the mutation status and expression of driver genes, especially for KRAS and SMAD4. Functional enrichment analysis identified the role of FLNB in the regulation of cell cycle, focal adhesion, vascular formation, and immune regulation. Knockdown of FLNB expression inhibited cancer cell proliferation and migration in-vitro and suppressed tumor growth in-vivo. Furthermore, FLNB overexpression caused high infiltration of Treg cells, Th2 cells, and TAMs, but reduced infiltration of $CD8^+$ T cells and Th1/Th2. Collectively, our findings suggest FLNB promotes PC progression and may be a novel biomarker for PC.

Keywords: Pancreatic cancer, FLNB, WGCNA, immune infiltration, prognosis, tumor microenvironment, TGF-β, immune-based therapy

Introduction

As one of the most aggressive malignancies, pancreatic cancer (PC) causes 4.5% of all cancer-related deaths worldwide in 2015 [1]. PC is widely recognized as a "cold" tumor and is highly immunosuppressive; thus, enhancing or recruiting anti-tumor immune cells into the tumor microenvironment (TME) is a promising therapeutic strategy for PC [2, 3]. In recent years, immune checkpoint inhibitors (ICIs) have been effectively used for several solid tumors, such as melanoma, non-small cell lung cancer, and hepatocellular carcinoma [4-7]. However, these drugs fail to demonstrate efficacy in patients with advanced PC due to the lack of $CD8^+$ T cells in the TME of PC [8-10]. Understanding the molecular mechanisms involved in PC immune suppression is therefore fundamental to the design of more effective immune-based therapeutics to improve the outcome of patients with PC.

Filamin B (FLNB) is a protein coding gene that interacts with glycoprotein Ib alpha as part of the process that repairs vascular injuries [11,

https://doi.org/10.62347/NUXC8231

12]. Early studies on FLNB focused on its mutation and its association with congenital abnormalities, such as Boomerang Dysplasia and Larsen syndrome [13-15]. Recent studies have found FLNB expression was negatively correlated with patients' survival in ovarian cancer and hepatocellular carcinoma [16, 17]. But the function of FLNB in cancer biology is largely unknown. Especially, the potential role of FLNB in pancreatic cancer has not been studied.

In the present study, we aimed at identifying a novel gene that is correlated with the immune cells that are associated with the prognosis of PC. To accomplish this, we used CIBERSORT algorithm to evaluate the immune landscape in PC based on the Cancer Genome Atlas (TCGA, https://cancergenome.nih.gov/) PC cohort. We then performed a weighted gene co-expression network analysis to identify FLNB as an important prognosis-associated gene. The potential association between the expression of FLNB and the infiltration levels of immune cells in PC was explored using CIBERSORT, single sample gene set enrichment analysis, and ESTIMATE algorithm.

Materials and methods

Data acquisition

The mRNA expression data was obtained based on fragments per kilobase million (FPKM). Corresponding clinical information from 177 patients with pancreatic cancer (PC) were obtained from the TCGA database in February 2020. Mutation data on KRAS, TP53, SMAD4, and CDKN2A in TCGG PC cohort were downloaded through cBioportal (TCGA provisional dataset). Of the 177 PC cases obtained, 171 were patients with overall survival (OS) >1 month. The following datasets were selected for further study: GSE62452, GSE60979, GSE28735, and GSE79668. We conducted our current study based the information in **Figure 1**. All datasets (TCGA, GSE62452, GSE60979, GSE28735 and GSE79668) are freely available as public resources. Therefore, local ethics approval was not needed.

Differential expression analysis

GSE62452 and GSE60979 were integrated into a meta-GEO PC cohort (73 non-tumor samples and 118 tumor samples), eliminating batch effects through the surrogate variable analysis (SVA) R package. The scale method of the limma R package [18] was used to normalize the data. A total of 18139 genes (mRNAs and lncRNAs) were involved in the mate-GEO PC cohort. Limma was also used to screen differentially expressed genes (DEGs) under the thresholds of false discovery rate (FDR) <0.05 and |log2 fold change (FC)| >0.1. The mRNAs in the TCGA PC cohort were screened through Limma with an average value greater than 1, and 14296 mRNAs were obtained and intersected with DEGs from the meta-GEO PC cohort to obtain one set of overlapped DEGs.

A CIBERSORT algorithm for TCGA PC cohort

With the help of the online calculator (https://cibersort.stanford.edu/), the CIBERSORT algorithm was used to estimate the infiltration level of 22 immune cell types in each TCGA PC sample [19]. The PC samples with *p*-value <0.05 and OS >1 month were selected for Kaplan-Meier (KM) survival analysis to screen prognosis-associated immune cells.

Weighted gene co-expression network analysis (WGCNA)

R package WGCNA was applied to construct co-expression modules and to detect overlapped DEGs co-expression modules that were significantly associated with the infiltration level of prognosis-associated immune cells in PC [20]. The soft threshold power was selected according to approximate scale-free topological power and was used to calculate the adjacency. We then transformed the adjacency matrix into a topological overlap matrix and used topological overlap (TOM) to describe the similarity of overlapped DEGs expression, and 1-TOM to show the heterogeneity between overlapped DEGs. Next, a hierarchical clustering tree was generated using the TOM. A dynamic tree was used to divide the modules of hierarchical clustering results, and to merge the modules with the number of overlapped DEGs <30 and cutting height <0.25. All modules were summarized by module eigengenes (ME), which were calculated to identify modules that were significantly associated with the infiltration level of prognosis-associated immune cells in PC. The module membership (MM) was defined as the correlation between overlapped DEG-expression values and the ME. Gene signifi-

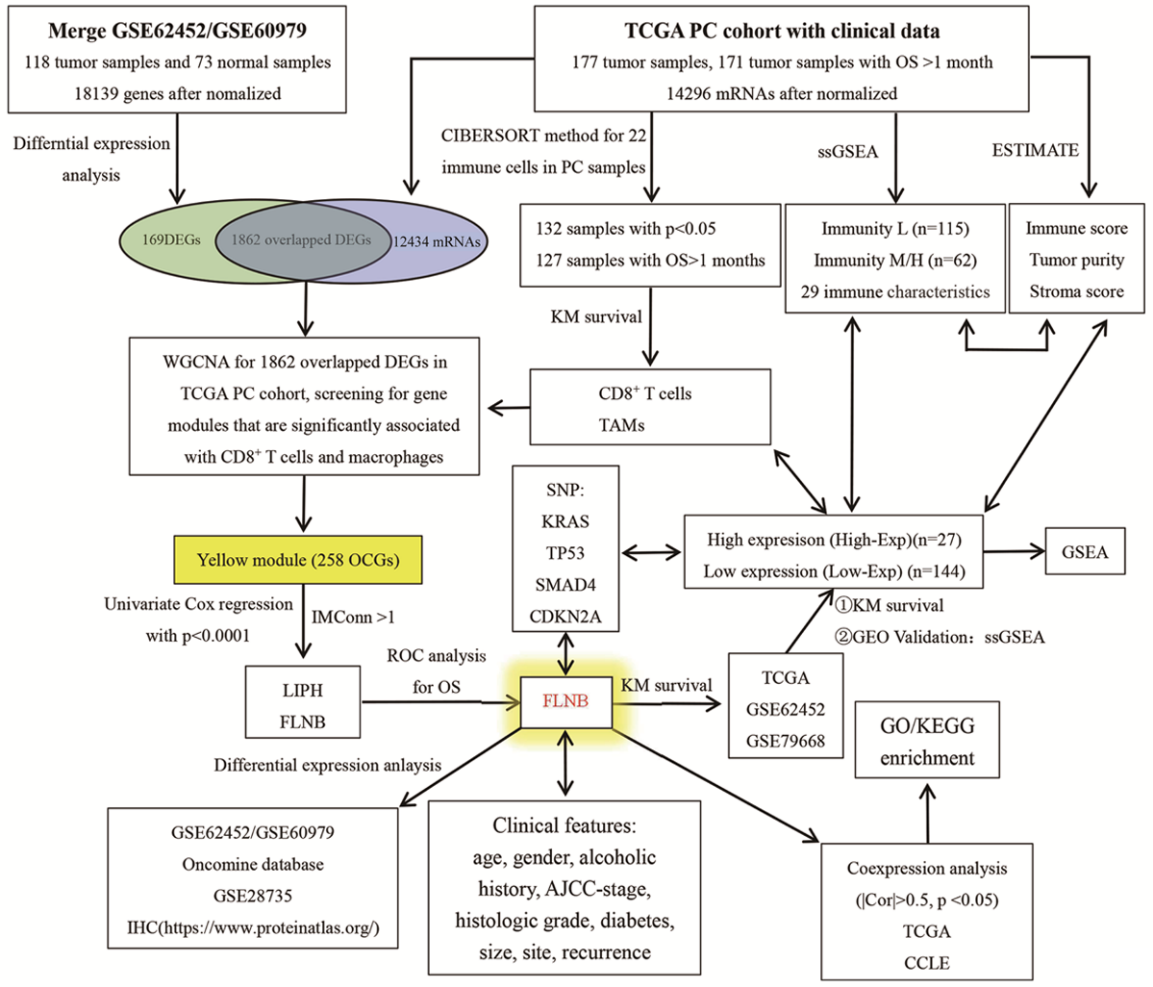

Figure 1. The flowchart of our study.

cance (GS) was defined as the correlation between the overlapped DEGs and the infiltration level of prognosis-associated immune cells. The intramodular connectivity (IMConn) was defined as the connectivity between an overlapped DEG and the other overlapped DEGs within a module. Subsequent analysis was performed based on the module that was the most relevant to the infiltration level of prognosis-associated immune cells in PC, which was considered as the immune-associated module.

Identification of FLNB as a prognosis-associated gene within the immune-associated module

The expression data of overlapped DEGs within the immune-associated module for 171 PC samples with OS >1 month and the corresponding clinical information were used to screen out the prognosis-associated genes using univariate Cox regression analysis (P<0.0001) with survival R package. Through the time ROC R package, receiver operating characteristic (ROC) curve analysis was performed for prognosis-associated genes with IMConn >1, among which FLNB had the highest area under the curve (AUC) of ROC curve analyses. Thus, we conducted subsequent studies to further explore FLNB.

Validation of the differential expression and the prognosis-association of FLNB through multiple datasets

Oncomine database (https://www.oncomine.org/resource/) was used to validate the differential expression of FLNB. Paired differential expression analysis of FLNB was performed based on GSE28735 dataset, which contained

the mRNA expression data of 45 pairs of pancreatic tumor and adjacent non-tumor tissues. The Human Protein Atlas database (http://proteinatlas.org/) was used to further validate the protein expression of FLNB. Survival analysis was performed separately to evaluate the association between the expression level of FLNB and OS of patients with PC in the TCGA, GSE62452, and GSE79668 cohorts. Patients in these three PC cohorts were respectively divided into low expression (low-Exp) and high expression (high-Exp) groups according to the optimal cutoff point obtained using the X-tile 3.6.1 software (Yale University, New Haven, CT, USA) and KM survival analysis was performed using the survminer R package [21].

Functional enrichment analysis

Gene set enrichment analysis (GSEA) (v3.0, http://software.broadinstitude.org/gsea/) was performed to evaluate the differences in potential biological pathways between the high- and low-Exp groups in the TCGA PC cohort. An annotated gene set c2.cp.kegg.6.2.symbols.gmt obtained from the Molecular Signatures Database (MSigDB) was selected for use as the reference gene set [22]. Genes significantly related to FLNB in the TCGA and the CCLE were screened out using Pearson correlation coefficients (Pearson correlated coefficient >0.5 or <-0.5, P<0.05). These FLNB correlated genes in each cohort were enrolled into ConsensuspathDB (http://cpdb.molgen.mpg.de/) and subjected to functional enrichment analysis; *p*-value <0.05 was considered significant [23].

Cell culture and transfection

Human PC cell lines, PANC-1 and Aspc-1 were purchased from the Cell Bank of the Chinese Academy of Science (Shanghai, China). Cells were cultured in RPMI-1640 medium (Invitrogen, Carlsbad, CA, USA) containing 10% fetal bovine serum (FBS; HyClone, Logan, UT, USA) and 1% penicillin/streptomycin in a humidified 5% CO_2 incubator at 37°C. Prior to transfection, cells were seeded onto 6-well plates with a density of 1×10^6 cells per well. At 80% confluence, small interfering RNA (siRNA) targeting FLNB and negative control siRNA (NC) were transfected into the cells using Lipofectamine 2000 (Invitrogen). Then, 48 hours after transfection, cells were collected for subsequent in-vitro functional analysis. The sequences (5'-3') of siRNA of FLNB were: siFLNB#1: sence: CCGGGCACAUAUGUGAUCUAUTT; antisence: AUAGAUCACAUAUGUGCCCGGTT; siFLNB#2: sence: GCCUUCAGGAAUCGGGAUUAATT; antisence: UUAAUCCCGAUUCCUGAAGGCTT.

Lentiviral shRNA knockdown

We synthesized two short hairpin RNA (shRNA) fragments specifically targeting human FLNB (Sangon Biotech, Shanghai, China) and inserted them into Mirzip lentiviral shRNA mir vectors (Open Biosystems, Lafayette, CO). These lentiviral plasmids were co-transfected with pVSVg, pRSV-Rev and pMDL into 293T cells using Lipofectamine 2000 (Invitrogen) to generate lentivirus. At 72 hours post-transfection, viral reservoirs were collected from transfected 293T cells and used to infect Aspc-1 cells with 10 μg/ml polypyrene. After infection, we add puromycin with 5 μg/ml in culture medium for 2 weeks to select stable cells. Viruses containing nonsense shRNA were used as controls. The shRNA knockdown subclones were used for animal studies. The sequences (5'-3') of shRNA of FLNB were: shFLNB#1: GCCTTCAGGAATCGGGATTAA; shFLNB#2: CCAGAAATCAACAGCAGTGAT.

MTT assay

Cell proliferation was measured using 3-(4,5-dimethylthiazal-2-yl)-2, 5-diphenyl-tetrazolium bromide (MTT) assay. Cells were cultured in 96-well plates at 2000 cell/well. At the indicated time points, 20 μL of MTT (5 mg/mL; Sigma-Aldrich, St. Louis, MO, USA) solution was added to each well and the plate was further incubated for 4 h. Culture supernatant was discarded and 100 μL DMSO (Corning Inc., Corning, NY, USA) was added to each well. Optical density (OD) was determined by measuring absorbance at 490 nm on a microplate reader (Bio-Tek Company, Winooski, VT, USA).

Plate clone formation assay

Cells were plated in 6-well plates (1000 cells/well, cultured for 10 days, and stained with 0.1% crystal violet). Colony forming units were counted under a microscope.

Sphere formation assay

Cells (1×10^3) were seeded in ultralow attachment 6-well plates (Corning) in DMEM/F12

(Gibco) supplemented with 20 μL/mL B27 (Gibco), 20 ng/mL epidermal growth factor (Gibco), and 20 ng/mL basic fibroblast growth factor (PeproTech, Hamada, Rehovot, Israel). After culture for one week, the number and diameters of spheres were determined under an inverted fluorescence microscope (Olympus, Tokyo, Japan).

Transwell invasion assays

Cell migration and invasion were examined using Transwell Permeable Supports (Corning Inc., Corning, NY, USA). Briefly, the transfected cells were allowed to grow to confluence. Cells (10^5) were suspended in 100 μL serum-free medium and plated in triplicates onto each 8 μm Transwell filter insert of 24-well plates coated with Matrigel (10 mg/L, BD Biosciences, San Jose, CA, USA). The lower chambers contained 10% fetal bovine serum. After 18 h, the cells in the upper chamber were removed with a cotton swab. The invasive cells at the bottom of the membrane were fixed with methanol and stained with 0.5% crystal violet for 20 min. The stained invaded cells were photographed under an inverted light microscope (magnification, ×100; Olympus Corp., Tokyo, Japan) and nine visual fields were observed in each group, respectively.

Western blot

Cells were collected and total proteins were lysed with RIPA buffer (Beyotime, Shanghai, China) and extracted. Protein concentration was determined using coomassie brilliant blue method (Beyotime, Shanghai, China). After denaturation, the total proteins were separated by sodium dodecyl sulfate-polyacrylamide gel electrophoresis (SDS-PAGE). Then, the proteins were transferred to polyvinylidene fluoride (PVDF) membrane (Merck, Burlington, MA, USA). The membrane was incubated incubated overnight at 4°C with primary antibodies after blocked with 5% milk. Next, the membrane was treated with anti-rabbit or anti-mouse secondary antibodies for 1 hour. Finally, the signal was detected were detected by an ECL Western blot kit (P06M31L, Gene-Protein Link, Beijing, China). Antibodies against E-Cadherin (1:1000 dilution, 20874-1-AP, Proteintech, Wuhan, China); Fibronectin (1:1000 dilution; ab32419, Abcam, Cambridge, MA, USA); Vimentin (1:5000 dilution, 10366-1-AP, Proteintech, Wuhan, China); α-SMA (1:2000 dilution; 23081-1-AP, Proteintech, Wuhan, China); Oct4 (1:5000 dilution, 20874-1-AP, Proteintech, Wuhan, China); GAPDH (1:10000 dilution; HRP-60004, Proteintech, Wuhan, China) and β-actin (1:10000 dilution; HRP-60008, Proteintech, Wuhan, China) were used as control.

Flow-cytometric analysis

The CD133 expression analyses were performed according to the instructions. Briefly, the fresh sorted $CD133^+$ cells were incubated at 4°C for 30 min with phycoerythrin (PE)-conjugated anti-human CD133/2 following treatment with FcR Blocking Reagent kit (from Miltenyi Biotec). Isotype-matched mouse IgG2b-PE antibodies served as controls. The data were analyzed by Windows 3.0 software (Beckman Coulter Life Sciences).

Immunohistochemical (IHC) staining and Immunofuorescence staining (IF)

IHC staining was performed using the standard streptavidin-biotin-peroxidase complex method. For IHC, the sections were incubated with specifc primary antibodies against E-cadherin (1:10000 dilution, 20874-1-AP, Proteintech, Wuhan, China), N-cadherin (1:2000 dilution, 22018-1-AP, Proteintech, Wuhan, China), Vimentin (1:5000 dilution, 10366-1-AP, Proteintech, Wuhan, China), Oct4 (1:5000 dilution, 20874-1-AP, Proteintech, Wuhan, China) and FLNB (1:200 dilution, 20685-1-AP, Proteintech, Wuhan, China) and then counterstained with hematoxylin. After staining, slides were scored under a microscope and analyzed for FLNB; E-cadherin; N-cadherin; Vimentin and Oct4 expression levels. IF was performed using an anti-FLNB antibody (1:50 dilution, 20685-1-AP, Proteintech, Wuhan, China).

Animal study

Male BALB/c nude mice (aged 4 weeks; n=5/group) were obtained from the Guangdong Provincial People's Hospital (Guangdong Academy of Medical Sciences). All the in vivo experiments were approved by the Committee on the Ethics of Animal Experiments of Guangdong Provincial People's Hospital (Guangdong Academy of Medical Sciences). For the xenograft experiments, the NC and sh-FLNB subclones (5×10^6 cells/mouse) of Aspc-1 cells

were resuspended in 100 μL RPMI-1640 and subcutaneously implanted in the right flank of the nude mice. Sample size of animal experiment was chosen according to similar conventions for well-designed experiments, and statistical methods were not used. The weight of the mice was assessed per 3 days. One month later, the mice were sacrificed, and tumors were harvested and weight.

Immune infiltration analysis for TCGA PC cohort

CIBERSORT algorithm was used to evaluate the differences in infiltration levels of prognosis-associated immune cells between the high- and low-Exp groups [19]. In the R package, single-sample gene set enrichment analysis (ssGSEA) was performed to quantify the activity or enrichment levels of immune cells, functions, or pathways in the cancer samples [24]. The following 29 immune-related terms were obtained: natural killer cells (NK cells), type-2 T helper cells (Th2 cells), type-1 T helper cells (Th1 cells), antigen-presenting cell (APC) co-stimulation, antigen-presenting cell (APC) co-inhibition, type-1 IFN response, major histocompatibility complex (MHC) class-1, parainflammation, plasmacytoid dendritic cells (pDCs), T cell co-stimulation, activated dendritic cells (aDCs), check-point, T cell co-inhibition, B cells, follicular helper T cells (Tfh), neutrophils, tumor-infiltrating lymphocyte (TIL), inflammation-promoting, $CD8^+$ T cells, cytolytic activity, type-1 IFN response, regulatory T cells (Treg), human leukocyte antigen (HLA), T helper cells, chemokine receptor (CCR), macrophages, mast cells, dendritic cells, immature dendritic cells (iDCs). Using the sparcl R package, the TCGA PC cohort was divided into three clusters-immunity L, immunity M, and immunity-according to the enrichment scores of the 29 immune-related terms. The ESTIMATE R package was subsequently used to assess the level of immune infiltration and tumor purity in the TCGA PC samples [25]. The immune score, which represents the infiltration of immune cells in tumor samples, was calculated for each PC sample in the TCGA PC cohort. PC samples with high tumor purity show low immune infiltration within tumors. And a higher immune score indicates a higher level of the infiltration of immune cells in tumor tissues. GSE62452 and GSE79668 cohorts were used to validate the immune infiltration landscape of PC through the ssGSEA method. Immune-related terms that differed between the high- and low-Exp groups in more than two cohorts were considered critical immune-related terms and selected for further analysis.

Statistical analysis

All statistical analyses were performed using R software (http:///www.r-project.org/), SPSS 25.0 software, and GraphPad prism 8.0 software (GraphPad Software, Inc.). Correlations were calculated using Pearson correlated coefficient. Group differences were analyzed by the Student's t-test and expressed as mean ± SD. All statistical tests were tow-sided; *p*-values <0.05 were considered as statistically significant.

Result

Differential expression analysis

We screened out 2031 DEGs from 18139 genes (mRNAs and lncRNAs) in the meta-GEO PC cohort under the thresholds of false discovery rate (FDR) <0.05 and |log2 fold change (FC)| >0.1 (Figure S1A). The 2031 DEGs were intersected with 14296 mRNAs from the TCGA PC cohort, resulting in 1862 overlapped DEGs (**Figure 1**).

Lower $CD8^+$ T cells infiltration or higher TAMs infiltration is associated with shorter overall survival in patients with PC

We used the CIBERSORT algorithm to estimate the infiltration level of 22 immune cell (IC) types in each TCGA PC sample. Cases with a CIBERSORT *P*-value of <0.05 were kept for further study. A total of 132 PC samples were selected, among which 127 PC had OS>1 month. KM survival analysis showed that patients with lower infiltration level of $CD8^+$ T cells or higher infiltration of TAMs had a worse OS (P<0.05) than those with higher infiltration of $CD8^+$ T cells or lower infiltration of TAMs (**Figures 1**, S1B, S1C).

WGCNA identifies FLNB as an unfavorable prognostic biomarker associated with the infiltration of $CD8^+$ T cell and TAM

To identify potential genes involved in infiltration of $CD8^+$ T cells and TAMs in PC, we conduct

WGCNA analysis by integrating the expression profile of 1862 overlapped DEGs and the infiltration level of $CD8^+$ T cells and TAMs. As shown in **Figure 2A** and **2B**, the soft-threshold power was set to 6, in which R^2 was 0.95, and this ensured a scale-free network. The soft-thresholding was determined to build the co-expression network. The minimum number of overlapped DEGs in the module was set to 30. We divided the initial module by dynamic tree shearing with the cutting height <0.25, and merge modules with high similarity of featured genes in the gene cluster dendrogram to obtain 10 modules (**Figure 2C**). All modules were summarized by module eigengenes (ME), which were calculated to identify modules that were significantly associated with the infiltration level of $CD8^+$ T cells in PC. Further, we created a heat map and found the highest correlation coefficient between yellow modules (258 overlapped DEGs) and the infiltration level of $CD8^+$ T cells and TAMs (Pearson Cor =-0.46 for $CD8^+$ T cells, Pearson Cor =0.43 for TAMs) (**Figures 1** and **2D**). We also drew module membership in the yellow module versus the infiltration level of $CD8^+$ T cells and TAMs to further reveal that the genes in the yellow modules were the most relevant to the infiltration level of $CD8^+$ T cells and TAMs (**Figure 2E**, **2F**).

Next, by using univariate Cox regression analysis for 258 overlapped DEGs within the yellow module (P<0.0001), we screened out seven prognosis-associated genes (LIPH, FLNB, AHNAK2, ANO1, EPS8, DSG2, and SFTA2) (**Table 1**), among which LIPH and FLNB were selected for ROC analysis under the threshold of IMConn>1 (**Figure 3A**). ROC analysis indicated that AUC of FLNB for OS was much higher than that of LIPH (**Figure 3B**, **3C**). Thus, FLNB was selected for subsequent analysis.

FLNB overexpression predicts poor prognosis in PC

To further analyze the predictive value of FLNB expression for survival, we first assessed its expression in PC tumor tissues as well as non-tumor normal tissues. We found that FLNB was overexpressed in PC in the meta-GEO PC cohort included in our study (P<0.0001) (**Figure 4A**). Gene expression analysis using the Oncomine database revealed that the expression of FLNB was also significantly higher in PC tissues (**Figure 4B-E**). Further, paired differential expression analysis based on GSE28735 cohort showed that the expression level of FLNB was much higher in PC tissues than that in the adjacent non-tumor tissue (P<0.0001) (**Figure 4F**). The results from the Human Protein Atlas database demonstrated that the protein expression of FLNB was significantly upregulated in tumor tissues (Figure S2). Importantly, KM survival analysis based on the TCGA PC cohort, GSE62452 cohort, and GSE79668 cohort revealed that patients with higher expression of FLNB had a worse OS than those with lower expression of FLNB (P<0.05). The groups were divided according to the best cutoff value of different datasets which obtained from survminer package by R (**Figure 4G-I**).

In the TCGA PC cohort, we found that the expression of FLNB was not statistically associated with age, alcohol consumption history, diabetes status, gender, tumor site, and the American Joint Committee on Cancer (AJCC) stage (Figure S3A-F). However, patients with larger tumors (size ≥4 cm) (P<0.05) or recurring disease (P<0.0001) had higher expression levels of FLNB (Figure S3G-I). Furthermore, in both the TCGA PC and GSE62452 cohorts, the expression of FLNB in PC samples with higher histologic grade was obviously higher than that in the PC samples with lower histologic grade (P<0.01) (Figure S3J). Taken together, these data suggest that FLNB overexpression was notably associated with poor prognosis in PC.

Association between FLNB expression and somatic mutation of PC driver gene

To investigate the mechanisms underlying FLNB erratic expression in PC, we evaluated the status of driver genes commonly mutated in PC. We found that KRAS, TP53, and CDKN2A mutation statuses were significantly associated with higher expression of FLNB, although not statistically significant for SMAD4 (**Figure 5A**). Differential expression analysis for these KRAS, TP53, CDKN2A, and SMAD4 in the high- and low-Exp FLNB groups in the TCGA PC cohort revealed that TP53 was not differentially expressed in the high-Exp group; however, KRAS and CDKN2A were upregulated in this group. In contrast, SMAD4 was significantly downregulated in the high-Exp group (**Figure 5B**), a finding which was also observed in the

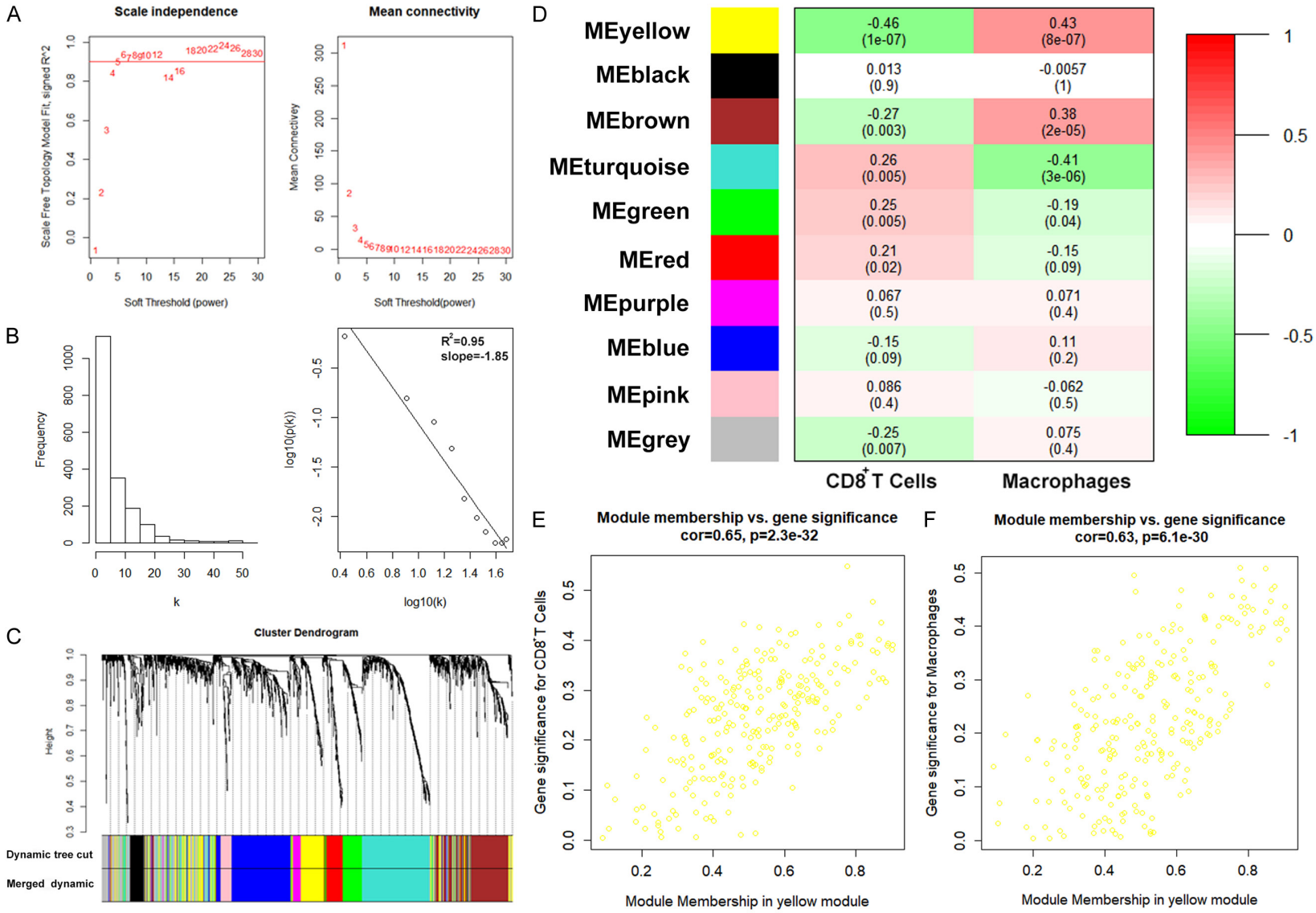

Figure 2. Weighted gene co-expression network analysis (WGCNA). A. Analysis of network topology for different soft-threshold power. B. Determination of soft-thresholding power in the WGCNA. C. Dynamic tree shearing with the cutting height <0.25, and merge modules with high similarity of featured genes. D. All modules were summarized by module eigengenes (ME) and heat map was conducted to identify modules that were significantly associated with the infiltration level of $CD8^+$ T cells in PC. E, F. The correlation of membership in the yellow module versus the infiltration level of $CD8^+$ T cells and TAMs.

Table 1. Univariate Cox regression analysis (P<0.0001) to screen out prognosis-associated genes

Gene	HR (95% CI)	*p*-value
AHNAK2	1.05 (1.03-1.08)	5.52E-05
ANO1	1.02 (1.01-1.03)	5.24E-06
DSG2	1.01 (1.01-1.02)	8.52E-05
EPS8	1.05 (1.03-1.07)	9.63E-06
FLNB	1.01 (1.00-1.01)	5.31E-05
LIPH	1.03 (1.01-1.05)	8.96E-05
SFTA2	1.01 (1.01-1.02)	1.82E-07

GSE62452 cohort (**Figure 5C**). Using cBioportal database, we also found that FLNB expression was positively correlated with KRAS expression (Cor =0.46, P=2.18e-10) (**Figure 5D**), while negatively correlated with SMAD4 expression (Cor =-0.36, P=1.523e-06) (**Figure 5E**). These results suggest that FLNB overexpression is associated with the mutation status and expression of driver genes, especially for KRAS and SMAD4, thereby indicating KRAS activation and SMAD4 inactivation in PC with FLNB overexpression.

Functional enrichment analysis of FLNB expression in PC

We further explored the activities of FLNB by analyzing its possible contributions to potential biological pathways in PC. We used GSEA to ask whether these pathways and their associated genes differ between the low-Exp and high-Exp FLNB groups (Figure S4A). We found that the cell cycle related gene set (NES = 2.19, FDR <0.05) was enriched in the high-Exp group (Figure S4A). We performed co-expression analysis (Pearson correlated coefficient >0.5 or <-0.5, P<0.05) for FLNB based on the TCGA PC cohort and CCLE database. Significantly correlated genes (413 co-expression genes in the TCGA PC cohort, and 130 co-expression genes in the CCLE database; see in Tables S1, S2) were enrolled into ConsensuspathDB (http://cpdb.molgen.mpg.de/) and subjected to functional enrichment analysis (P<0.05) (Figure S4B). We found that these genes were consistently enriched in the TCGA PC cohort as well as in the CCLE database. GO enrichment analysis revealed that FLNB may play an important role in cellular response to cytokine stimulus and contractile actin filament bundle (Figure S4B). Furthermore, pathway enrichment analysis showed that FLNB may be involved in vascular formation (VEGFA-VEGFR2 signaling pathway), focal adhesion, and immune regulation (such as TCR) (Figure S4B). These results implied that FLNB overexpression provides necessary support for tumor growth and immune regulation of PC.

FLNB knockdown suppresses the proliferation and the invasion of PC cells lines

To further evaluate the functional role of FLNB in tumor cells proliferation and invasion, we transfected PANC-1 and AsPC-1 cells with si-FLNB. Abrogated levels of FLNB in these two cells were validated using WB and RT-qPCR analysis (P<0.0001) (**Figure 6A**, **6B**). Using the MTT assay, we found that cell proliferation was significantly inhibited in FLNB-depleted PANC-1 and AsPC-1 cells (P<0.0001) (**Figure 6C**). In the plate colony formation assay, the number of colonies in the si-FLNB groups was significantly lower than that in the NC (control) group (P<0.0001) (**Figure 6D**). Moreover, the transwell assay performed to determine the invasive capacity of PANC-1 and AsPC-1 cells transfected with si-FLNB revealed that the number of invasion cells was significantly less in the si-FLNB groups than that in the NC group (P<0.0001) (**Figure 6E**). Moreover, the FLNB expression was further determined by IF in pairs of PDAC and non-tumor specimens (**Figure 6F**). These data suggest FLNB is necessary for cancer cell proliferation and invasion in PC.

FLNB knockdown suppresses tumor growth and the stemness of PC cells

In vitro experiments demonstrated that FLNB knockdown suppressed the proliferation. We designed in vivo experiments to further confirm its function. We generated two sh-FLNB subclones of Aspc-1 cells and chose sh-FLNB#2 with higher knockdown efficiency for subsequent experiments. The results showed that FLNB knockdown significantly decreased tumor volume (**Figure 7A**, **7B**) and weight (**Figure 7C**) compared to those of controls. The Sphere Formation Efficiency also decreased in sh-FLNB group (**Figure 7D**). To further explore the role of FLNB in tumor stemness, we conducted Flow cytometry and found sh-FLNB group inhibited cell stemness compared with NC group (**Figure 7E**). Further, we detected the effect of FLNB on the expression of EMT-related and

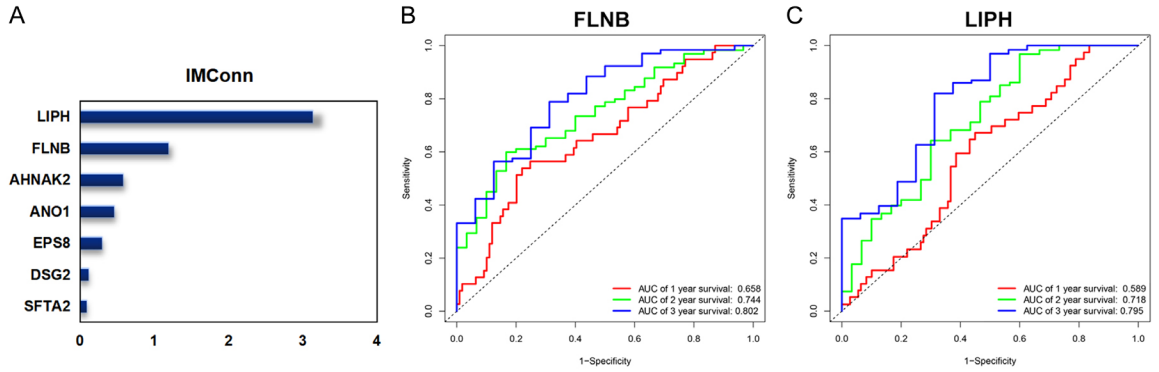

Figure 3. Identification of FLNB as key OCG (KOCG) from PAIM. A. The IMConn of seven PAGs (LIPH, FLNB, AHNAK2, ANO1, EPS8, DSG2, and SFTA2). B. Time-dependent ROC analysis for FLNB. C. Time-dependent ROC analysis for LIPH.

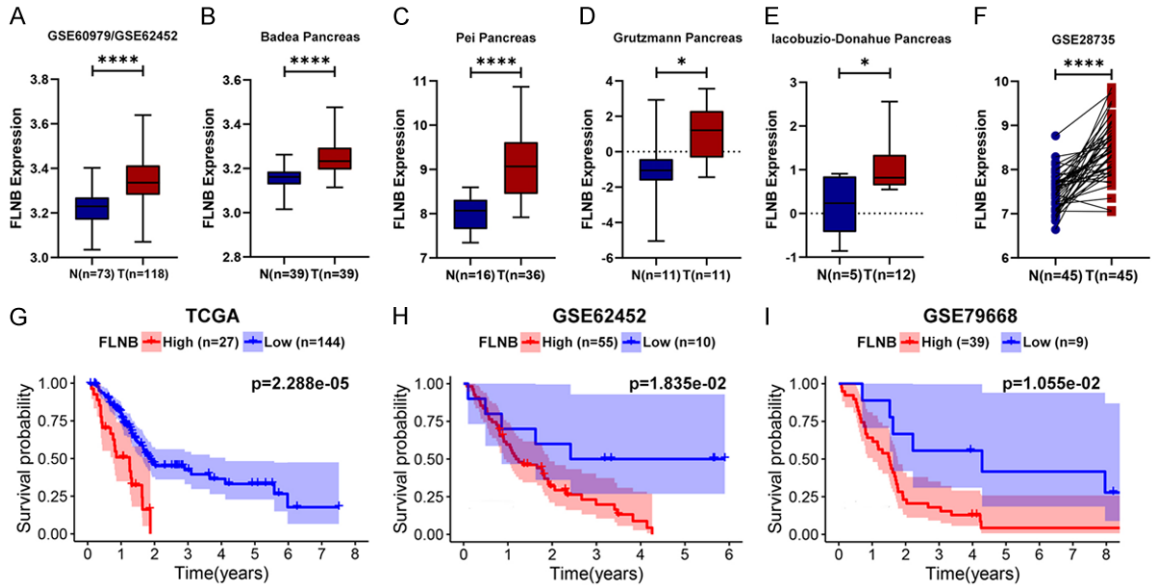

Figure 4. Validation of the differential expression and the prognosis association of FLNB in multiple datasets. A-F. Differential expression analysis for FLNB using multiple datasets. G-I. KM survival analysis for FLNB through the TCGA, GSE62425, and GSE79668 cohorts. FLNB overexpression was significantly associated with poor survival in PC (*P<0.05; **P<0.01; ***P<0.001; ****P<0.0001).

stemness genes, sh-FLNB decreased the expression of Fibronectin, Vimentin, α-SMA and Oct4 with control cells (**Figure 7F**). In addition, as shown by IHC staining, sh-FLNB significantly decreased the expression of EMT and stemness (**Figure 7G**). These results demonstrate that FLNB was important in tumor stemness and regulating the expression of EMT target genes.

FLNB overexpression promotes immune suppression or evasion of PC

Based on CIBERSORT analysis, we found that the infiltration level of $CD8^+$ T cells was lower in the high-Exp group (P<0.05) (**Figure 8A**). In contrast, higher infiltration level of TAMs in the high-Exp group was observed (**Figure 8B**). TAMs had much higher proportion within tumor than $CD8^+$ T cells. From the ssGSEA data, the enrichment scores of 29 immune-related term were obtained and 177 PC samples in the TCGA PC cohort were divided into immunity L (n=115), immunity M (n=55), and immunity H (n=7) (**Figure 8C**). We merged immunity M and immunity H into immunity M/H (n=62) and found that the expression level of FLNB in immunity M/H was much lower than that in immunity L (P<0.05) (**Figure 8D**). Tumor purity in the high-Exp group was also much higher

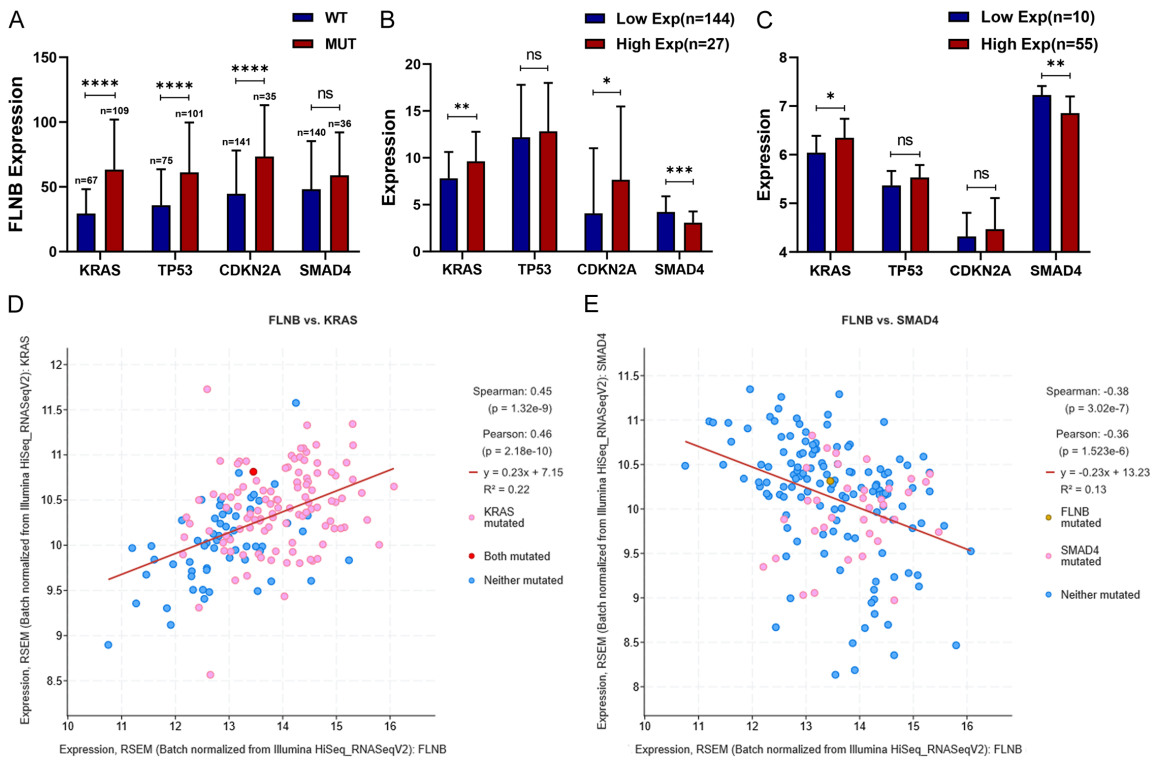

Figure 5. Association between FLNB expression and somatic mutations in PC. A. The KRAS, TP53, and CDKN2A mutation statuses were significantly associated with FLNB expression, while SMAD4 mutation status was not correlated with FLNB expression. B. Differential expression analysis of KRAS, TP53, CDKN2A, and SMAD4 in high- and low-Exp groups in the TCGA PC cohort. TP53 was not differentially expressed, while KRAS and CDKN2A were upregulated in the high-Exp group, and SMAD4 was significantly downregulated in the high-Exp group. C. Differential expression analysis of KRAS, TP53, CDKN2A, and SMAD4 between the high- and low-Exp groups in the GSE79668 cohort. KRAS was significantly upregulated in the high-Exp group and SMAD4 was significantly downregulated in the low-Exp group. D, E. Correlation analysis between FLNB, KRAS, and SMAD4 in cBioportal database (*P<0.05; **P<0.01; ***P<0.001; ****P<0.0001).

compared with that in the low-Exp group (P<0.01) (**Figure 8E**), while immune score in the high-Exp group was lower compared with that in the low-Exp group (P<0.01) (**Figure 8F**). As presented in **Figure 8G**, in the TCGA PC cohort, $CD8^+$ T cells, TILs, cytolytic activity, check point, T helper cells, Th1 cells, Th1/Th2, and HLA were enriched in the low-Exp group. In contrast, Th2 cells were enriched in the high-Exp group (P<0.05) (**Figure 8G**); similar results were observed in the GSE62452 cohort (P<0.05) (Figure S5A). In the GSE62452 cohort, we also found that the enriched level of $CD8^+$ T cells and Th1/Th2 within tumors in the low-Exp group were significantly higher than those in the high-Exp group (P<0.05). Moreover, tumors with high FLNB expression were significantly associated high enriched levels of TAMs and Treg cells in both GSE62452 and GSE79668 cohorts (P<0.05) (Figure S5A, S5B). In summary, these results demonstrated that FLNB overexpression was significantly associated with low infiltration levels of $CD8^+$ T cells and Th1/Th2 within tumors, and high infiltration levels of Treg cells, Th2 cells, and TAMs, thereby promoting immune suppression or evasion.

Discussion

In the current study, we identified FLNB as a critical oncogene which might regulate immune suppression and tumor progression in PC. Through the data mining of multiple databases, our study has shown that FLNB overexpression is significantly associated with low infiltration of $CD8^+$ T cells and high infiltration of TAMs. Moreover, FLNB expression positively correlated with histologic grade, tumor recurrence, tumor size, and poor survival in PC. And FLNB knockdown inhibited cell proliferation and invasion in PC cell. Thus, our work first demon-

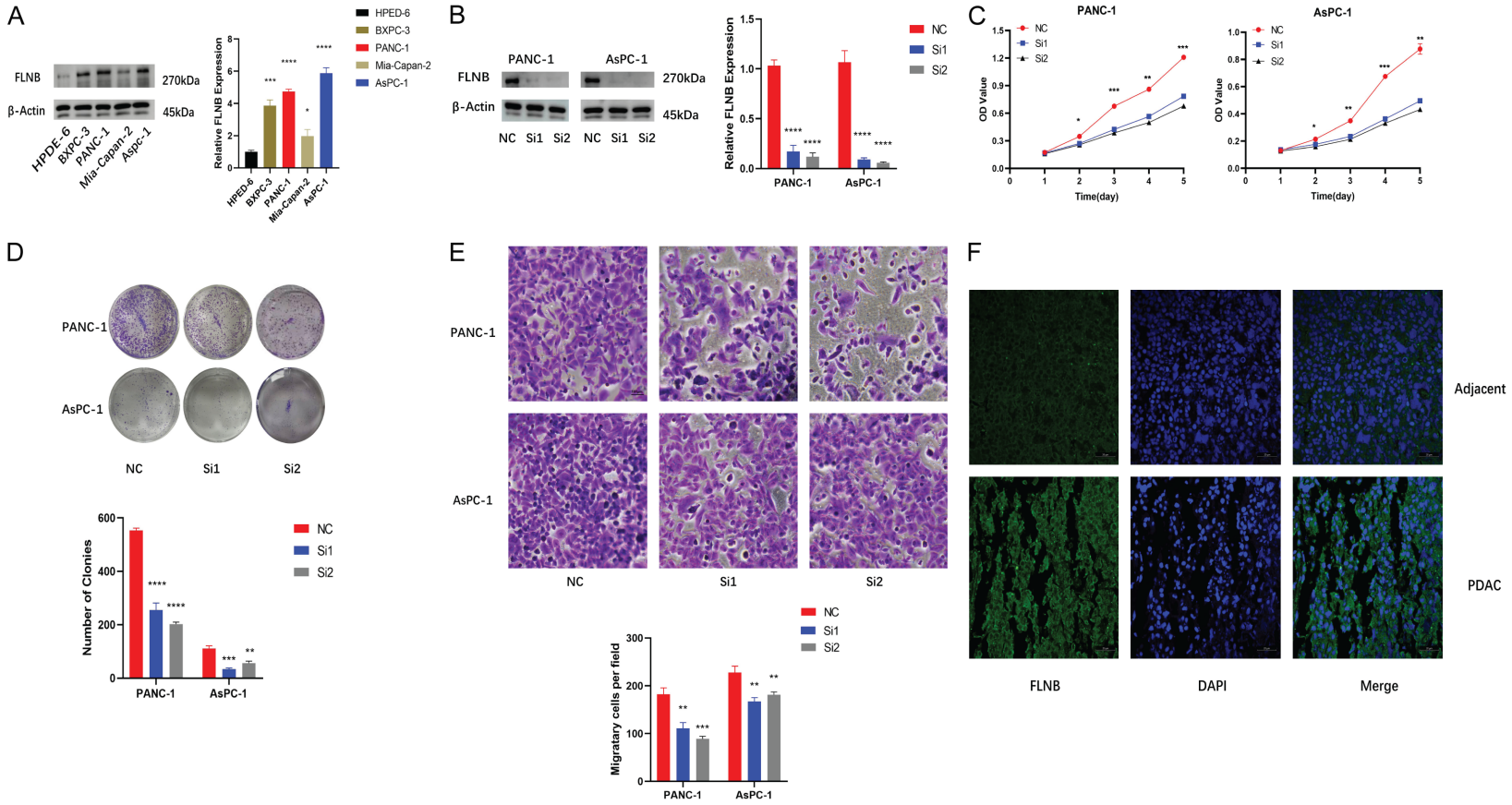

Figure 6. FLNB knockdown suppresses the proliferation and invasion of PC cells lines. A. WB and RT-PCR analysis of different cell lines of PDAC. B. WB and RT-PCR analysis validated the knockdown of FLNB in PANC-1 and AsPC-1 cells transfected with control siRNA (NC) or si-FLNB. C. Assessment of cell proliferation using the MTT assay. D. Colony formation assay was used to determine the colony-formation ability of PANC-1 and AsPC-1 cells transfected with si-FLNB. E. Transwell assay was performed to determine the invasive capacity of PANC-1 and AsPC-1 cells transfected with si-FLNB. F. Representative images of IF of FLNB (green) in PDAC and adjacent normal tissues. DAPI (blue) was used for nuclear counterstaining. Scale bar =20 μm (*P<0.05; **P<0.01; ***P<0.001; ****P<0.0001).

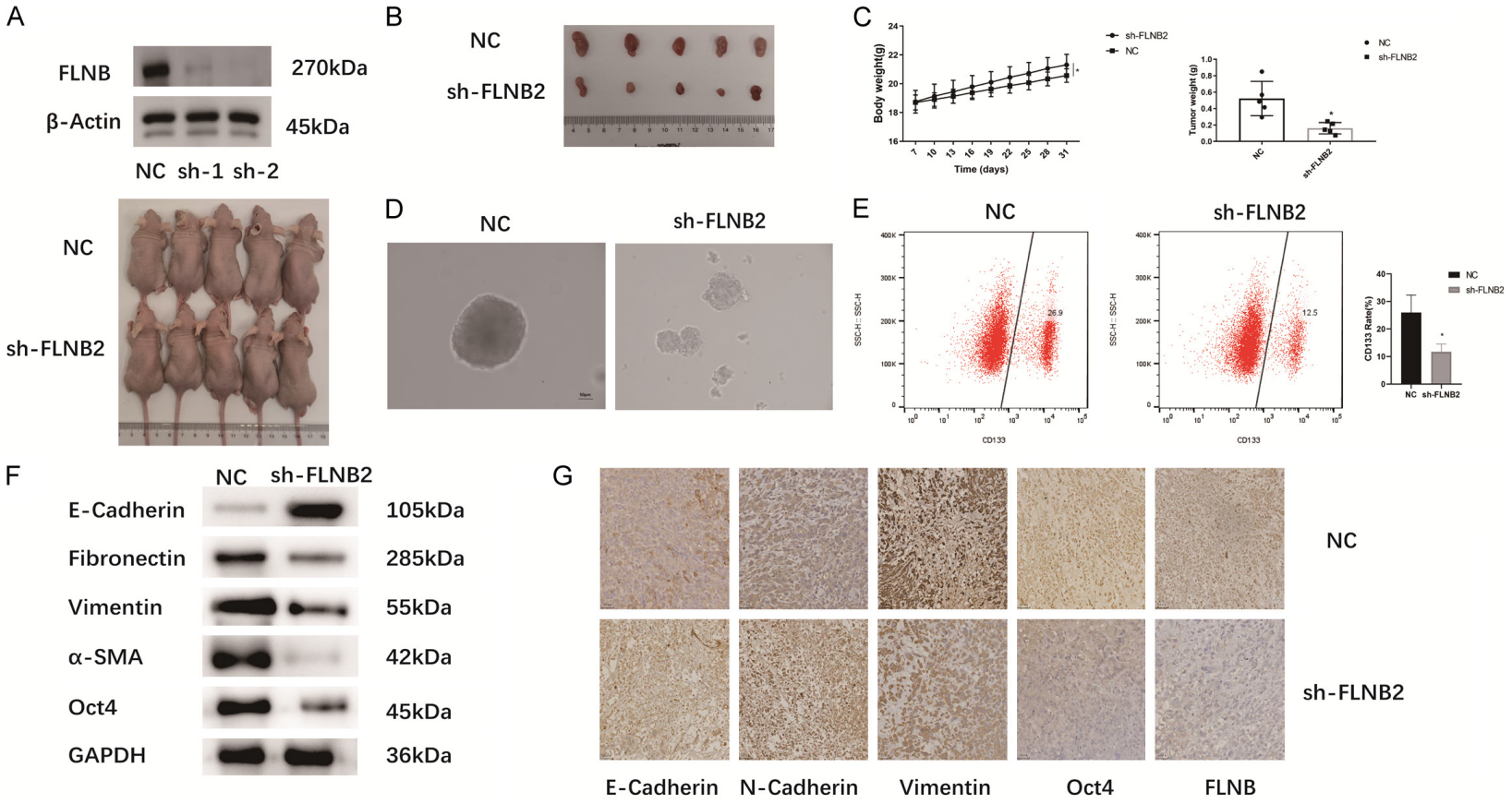

Figure 7. FLNB knockdown suppresses tumor growth and the stemness of PC cells. A, B. Tumor size is shown in FLNB konckdown groups and the control groups. C. Body weight of mice were measured every 3 days after injection with human PC lines and compared with controls. Tomor weight were measured of FLNB konckdown groups and the control groups. D. The Sphere Formation assay was used to determine the Sphere Formation Efficiency of PC cells transfected with control siRNA (NC) or si-FLNB. E. Flow cytometric analysis of control siRNA (NC) or si-FLNB, indicating si-FLNB group significantly inhibited cell stemness. F. The protein levels of EMT-related and stemness genes were determined in control siRNA (NC) or si-FLNB. GAPDH used as internal control. G. Representative images of IHC staining of two groups. Scale bar =50 μm (*P<0.05; **P<0.01; ***P<0.001; ****P<0.0001).

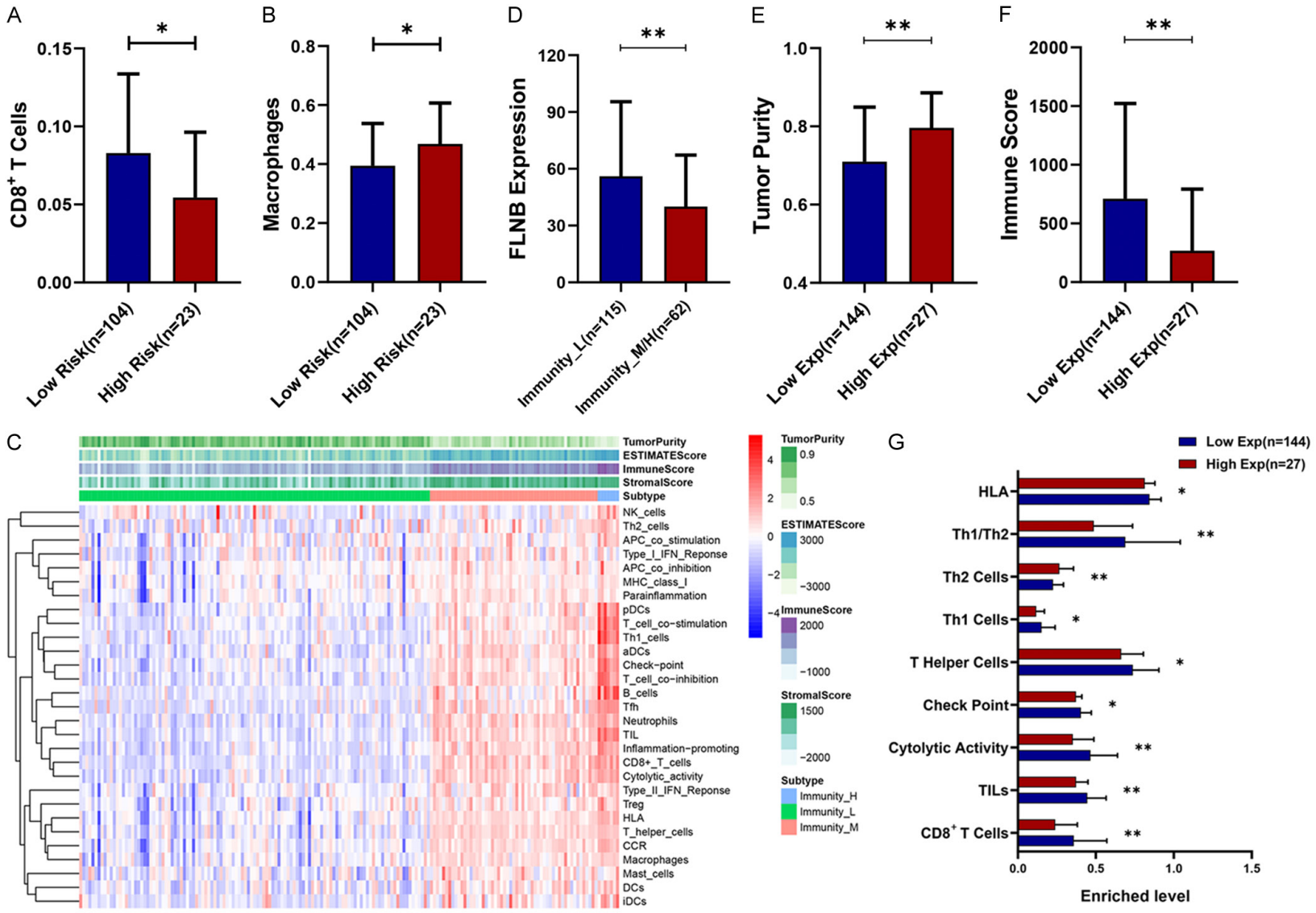

Figure 8. Association between FLNB expression and the immune infiltration within tumor in the TCGA cohort. A. CIBERSORT algorithm demonstrated that FLNB expression was negatively associated with infiltration of $CD8^+$ T cell within the tumor. B. The CIBERSORT algorithm demonstrated that FLNB expression was positively associated with the infiltration of TAMs. C. Based on the ssGSEA analysis, the enrichment scores of 29 immune-related term were obtained and 177 PC samples in

the TCGA PC cohort were divided into the immunity L (n=115), immunity M (n=55), and immunity H (n=7) groups. D. FLNB expression was significantly upregulated in the immunity-L group compared with the immunity-M/H groups. E. The ESTIMATE algorithm demonstrated that tumor purity was significantly upregulated in the high-Exp group than that in the low-Exp group. F. The ESTIMATE algorithm demonstrated that the immune score was significantly downregulated in the high-Exp group than that in the low-Exp group. G. The ssGSEA algorithm demonstrated that $CD8^+$ T cells, TILs, cytolytic activity, check point, T helper cells, Th1 cells, Th1/Th2, and HLA were enriched in the low-Exp group, while Th2 cells were enriched in the high-Exp group (*P<0.05; **P<0.01; ***P<0.001; ****P<0.0001).

strates the role of FLNB in promoting tumor progression and immune suppression and in predicting patients' prognosis in PC.

Through GSEA, we found that FLNB might be involved in the regulation of cell cycle. Furthermore, GO and pathway enrichment analysis based on TCGA PC cohort and CCLE databases revealed that FLNB plays a role in the regulation of contractile actin filament bundle, cellular response to cytokine stimulus and focal adhesion, which are also involved in cell division. Of note, we also demonstrated that knockdown of FLNB inhibited the proliferation and invasion capacity of pancreatic cancer cells. Taken together, these results suggest that FLNB could promote PC cell proliferation by affecting the cell division process via regulation of cell cycle. TGF-β/SMAD signaling has been reported to suppress tumor formation by blocking cell cycle progression and maintaining tissue hemostasis [26, 27]. In PC, SMAD4 is commonly mutated and inactivated, which impairs tumor suppressive function of TGF-β and cause tumor development [28]. In our study, we found that FLNB overexpression was significantly associated with SMAD4 mutation (although not statistically significant) and low expression of SMAD4. Thus, we propose that FLNB overexpression induced SMAD4 inactivation, leading to unlimited active cell division cycle. It will be of interest to design further experimental studies to investigate the detailed mechanism by which FLNB regulates mitotic cycle in PC.

In the current study, we demonstrate that an increasing number of $CD8^+$ T cells are associated with significantly prolonged survival in PC. However, the infiltration of $CD8^+$ T cells is relatively rare in the TME of PC. A high number of tumor-associated immunosuppressive cells (e.g. TAMs and Treg cells) function as a barrier to $CD8^+$ T cells infiltration [29]. Consistently, our data showed that the proportion of $CD8^+$ T cells within tumors is much less than that of TAMs, indicating that high infiltration of TAMs within tumor may decrease the infiltration of $CD8^+$ T cells. Previous reports have also shown that the tumor immune-exhausted status could be reverted by blocking immune checkpoints with monoclonal antibodies; a significant number of preexisting $CD8^+$ T cells in TME is however required for an efficient response to ICIs [30-32]. Thus, patients with PC in the FLNB low-Exp group may be more sensitive to ICIs compared to those in the high-Exp group, owing to a limited infiltration of $CD8^+$ T cells in the TME in high-Exp group. Moreover, since FLNB was responsible for decreased $CD8^+$ T cells, it might be interesting to test whether combination with FLNB inhibitor and ICIs could have effect on synergy effect in PC.

One of the most important factors though which FLNB contribute to immune suppression is KRAS mutation. Existing studies have reported that KRAS-mutated cancer cells help to build the immunosuppressive environment by modulating immune cell behavior or function in PC [33]. For example, KRAS mutated cancer cells have been reported to secrete granulocyte-macrophage, the colony-stimulating factor (GM-CSF), and recruit myeloid-derived suppressor cells, which suppress the infiltrating and antitumor activities of $CD8^+$ cytotoxic T cells [34]. Additional studies have also shown that oncogenic KRAS impairs MHC-I of the antigen presentation pathway, allowing evasion of tumor-infiltrating lymphocytes [35]. Moreover, KRAS mutation was also involved in promoting Treg recruitment and TAMs polarization, and subsequently contributes to immunosuppression in the TME [36]. Interestingly, we showed a high expression of FLNB is associated with KRAS mutation and higher KRAS expression. Based on these, we propose that FLNB overexpression and KRAS activation together induce immune suppression or evasion in PC.

Our study provides new insights into the PC immune microenvironment and immune-based therapies by providing clear evidence for an oncogenic role of FLNB in PC. In particular, we

describe the FLNB related immune cell phenotype in PC. However, the study has some limitations. Firstly, this is a retrospective study based on publicly available datasets; thus, the quality of data may influence study outcomes. Secondly, the potential role of FLNB in pancreatic carcinogenesis was validated *in vitro*, but not *in vivo*. Hence, further experimental studies should be performed to elucidate the regulative mechanism between FLNB and immune cells in PC.

In summary, our findings showed that FLNB overexpression promoted tumor progression and was associated with the immune suppressive phenotype. Thus, we established FLNB as a novel prognostic biomarker, which identifies it as a novel potential therapeutic target in PC.

Acknowledgements

This study was supported by National Natural Science Foundation of China (82072635), High-level Hospital Construction Research Project of Heyuan People's Hospital (YNKT202202), the Science and Technology Program of Heyuan [23051017147335].

Disclosure of conflict of interest

None.

Address correspondence to: Dr. Baohua Hou, Department of General Surgery, Guangdong Provincial People's Hospital (Guangdong Academy of Medical Sciences), Southern Medical University, Guangzhou, Guangdong, China. E-mail: hbh1000@126.com; Dr. Qing Gou, Department of Interventional Radiology, Guangdong Provincial People's Hospital (Guangdong Academy of Medical Sciences), Southern Medical University, Guangzhou, Guangdong, China. E-mail: gouqinger@126.com; Dr. Hongkai Zhuang, Sun Yat-sen University Cancer Center, Guangzhou, Guangdong, China. E-mail: 79900-2305@qq.com

References

[1] Kamisawa T, Wood LD, Itoi T and Takaori K. Pancreatic cancer. Lancet 2016; 388: 73-85.

[2] Bazhin AV, Shevchenko I, Umansky V, Werner J and Karakhanova S. Two immune faces of pancreatic adenocarcinoma: possible implication for immunotherapy. Cancer Immunol Immunother 2014; 63: 59-65.

[3] Elaileh A, Saharia A, Potter L, Baio F, Ghafel A, Abdelrahim M and Heyne K. Promising new treatments for pancreatic cancer in the era of targeted and immune therapies. Am J Cancer Res 2019; 9: 1871-1888.

[4] Cervello M, Emma MR, Augello G, Cusimano A, Giannitrapani L, Soresi M, Akula SM, Abrams SL, Steelman LS, Gulino A, Belmonte B, Montalto G and McCubrey JA. New landscapes and horizons in hepatocellular carcinoma therapy. Aging (Albany NY) 2020; 12: 3053-3094.

[5] Schouwenburg MG, Suijkerbuijk KPM, Koornstra RHT, Jochems A, van Zeijl MCT, van den Eertwegh AJM, Haanen JBAG, Aarts MJ, Akkooi ACJV, Berkmortel FWPJVD, Groot JWB, Hospers GAP, Kapiteijn E, Kruit WH, Piersma D, van Rijn RS, Ten Tije AJ, Vreugdenhil G, Hoeven JJMV and Wouters MWJM. Switching to immune checkpoint inhibitors upon response to targeted therapy; the road to long-term survival in advanced melanoma patients with highly elevated serum LDH? Cancers (Basel) 2019; 11: 1940.

[6] Ridolfi L, De Rosa F, Petracci E, Tanda ET, Marra E, Pigozzo J, Marconcini R, Guida M, Cappellini GCA, Gallizzi G, Occelli M, Pala L, Gambale E, Bersanelli M, Galdo G, Cortellini A, Morgese F, Zoratto F, Stucci LS, Strippoli S and Guidoboni M; Italian Melanoma Intergroup (IMI). Anti-PD1 antibodies in patients aged ≥ 75 years with metastatic melanoma: a retrospective multicentre study. J Geriatr Oncol 2020; 11: 515-522.

[7] Fu Y, Liu S, Zeng S and Shen H. From bench to bed: the tumor immune microenvironment and current immunotherapeutic strategies for hepatocellular carcinoma. J Exp Clin Cancer Res 2019; 38: 396.

[8] Balachandran VP, Beatty GL and Dougan SK. Broadening the impact of immunotherapy to pancreatic cancer: challenges and opportunities. Gastroenterology 2019; 156: 2056-2072.

[9] Li J, Yuan S, Norgard RJ, Yan F, Yamazoe T, Blanco A and Stanger BZ. Tumor cell-intrinsic USP22 suppresses antitumor immunity in pancreatic cancer. Cancer Immunol Res 2020; 8: 282-291.

[10] Hou YC, Chao YJ, Hsieh MH, Tung HL, Wang HC and Shan YS. Low CD8+ T cell infiltration and high PD-L1 expression are associated with level of CD44+/CD133+ cancer stem cells and predict an unfavorable prognosis in pancreatic cancer. Cancers (Basel) 2019; 11: 541.

[11] Bandaru S, Zhou AX, Rouhi P, Zhang Y, Bergo MO, Cao Y and Akyürek LM. Targeting filamin B induces tumor growth and metastasis via enhanced activity of matrix metalloproteinase-9 and secretion of VEGF-A. Oncogenesis 2014; 3: e119.

[12] Su YT, Gao C, Liu Y, Guo S, Wang A, Wang B, Erdjument-Bromage H, Miyagi M, Tempst P and Kao HY. Monoubiquitination of filamin B

regulates vascular endothelial growth factor-mediated trafficking of histone deacetylase 7. Mol Cell Biol 2013; 33: 1546-1560.
[13] Bicknell LS, Morgan T, Bonafé L, Wessels MW, Bialer MG, Willems PJ, Cohn DH, Krakow D and Robertson SP. Mutations in FLNB cause boomerang dysplasia. J Med Genet 2005; 42: e43.
[14] Xu Q, Wu N, Cui L, Lin M, Thirumal Kumar D, George Priya Doss C, Wu Z, Shen J, Song X and Qiu G. Comparative analysis of the two extremes of FLNB-mutated autosomal dominant disease spectrum: from clinical phenotypes to cellular and molecular findings. Am J Transl Res 2018; 10: 1400-1412.
[15] Bernkopf M, Hunt D, Koelling N, Morgan T, Collins AL, Fairhurst J, Robertson SP, Douglas AGL and Goriely A. Quantification of transmission risk in a male patient with a FLNB mosaic mutation causing Larsen syndrome: implications for genetic counseling in postzygotic mosaicism cases. Hum Mutat 2017; 38: 1360-1364.
[16] Li J, Zhang S, Wu L and Pei M. Interaction between LncRNA-ROR and miR-145 contributes to epithelial-mesenchymal transition of ovarian cancer cells. Gen Physiol Biophys 2019; 38: 461-471.
[17] Kim H, Kim K, Yu SJ, Jang ES, Yu J, Cho G, Yoon JH and Kim Y. Development of biomarkers for screening hepatocellular carcinoma using global data mining and multiple reaction monitoring. PLoS One 2013; 8: e63468.
[18] Ritchie ME, Phipson B, Wu D, Hu Y, Law CW, Shi W and Smyth GK. limma powers differential expression analyses for RNA-sequencing and microarray studies. Nucleic Acids Res 2015; 43: e47.
[19] Newman AM, Liu CL, Green MR, Gentles AJ, Feng W, Xu Y, Hoang CD, Diehn M and Alizadeh AA. Robust enumeration of cell subsets from tissue expression profiles. Nat Methods 2015; 12: 453-457.
[20] Langfelder P and Horvath S. WGCNA: an R package for weighted correlation network analysis. BMC Bioinformatics 2008; 9: 559.
[21] Camp RL, Dolled-Filhart M and Rimm DL. X-tile: a new bio-informatics tool for biomarker assessment and outcome-based cut-point optimization. Clin Cancer Res 2004; 10: 7252-7259.
[22] Subramanian A, Tamayo P, Mootha VK, Mukherjee S, Ebert BL, Gillette MA, Paulovich A, Pomeroy SL, Golub TR, Lander ES and Mesirov JP. Gene set enrichment analysis: a knowledge-based approach for interpreting genome-wide expression profiles. Proc Natl Acad Sci U S A 2005; 102: 15545-15550.
[23] Kamburov A, Stelzl U, Lehrach H and Herwig R. The ConsensusPathDB interaction database: 2013 update. Nucleic Acids Res 2013; 41: D793-D800.
[24] Hänzelmann S, Castelo R and Guinney J. GSVA: gene set variation analysis for microarray and RNA-seq data. BMC Bioinformatics 2013; 14: 7.
[25] Yoshihara K, Shahmoradgoli M, Martínez E, Vegesna R, Kim H, Torres-Garcia W, Treviño V, Shen H, Laird PW, Levine DA, Carter SL, Getz G, Stemke-Hale K, Mills GB and Verhaak RG. Inferring tumour purity and stromal and immune cell admixture from expression data. Nat Commun 2013; 4: 2612.
[26] Chen Y, Di C, Zhang X, Wang J, Wang F, Yan JF, Xu C, Zhang J, Zhang Q, Li H, Yang H and Zhang H. Transforming growth factor β signaling pathway: a promising therapeutic target for cancer. J Cell Physiol 2020; 235: 1903-1914.
[27] Fang P, Li X, Dai J, Cole L, Camacho JA, Zhang Y, Ji Y, Wang J, Yang XF and Wang H. Immune cell subset differentiation and tissue inflammation. J Hematol Oncol 2018; 11: 97.
[28] Ahmed S, Bradshaw AD, Gera S, Dewan MZ and Xu R. The TGF-β/Smad4 signaling pathway in pancreatic carcinogenesis and its clinical significance. J Clin Med 2017; 6: 5.
[29] Jiang H, Hegde S, Knolhoff BL, Zhu Y, Herndon JM, Meyer MA, Nywening TM, Hawkins WG, Shapiro IM, Weaver DT, Pachter JA, Wang-Gillam A and DeNardo DG. Targeting focal adhesion kinase renders pancreatic cancers responsive to checkpoint immunotherapy. Nat Med 2016; 22: 851-860.
[30] Chow MT, Ozga AJ, Servis RL, Frederick DT, Lo JA, Fisher DE, Freeman GJ, Boland GM and Luster AD. Intratumoral activity of the CXCR3 chemokine system is required for the efficacy of Anti-PD-1 therapy. Immunity 2019; 50: 1498-1512.
[31] Figueroa-Protti L, Soto-Molinari R, Calderón-Osorno M, Mora J and Alpízar-Alpízar W. Gastric cancer in the era of immune checkpoint blockade. J Oncol 2019; 2019: 1079710.
[32] Spranger S, Koblish HK, Horton B, Scherle PA, Newton R and Gajewski TF. Mechanism of tumor rejection with doublets of CTLA-4, PD-1/PD-L1, or IDO blockade involves restored IL-2 production and proliferation of CD8(+) T cells directly within the tumor microenvironment. J Immunother Cancer 2014; 2: 3.
[33] Cullis J, Das S and Bar-Sagi D. Kras and tumor immunity: friend or foe? Cold Spring Harb Perspect Med 2018; 8: a031849.
[34] Bayne LJ, Beatty GL, Jhala N, Clark CE, Rhim AD, Stanger BZ and Vonderheide RH. Tumor-derived granulocyte-macrophage colony-stimu-

lating factor regulates myeloid inflammation and T cell immunity in pancreatic cancer. Cancer Cell 2012; 21: 822-835.

[35] El-Jawhari JJ, El-Sherbiny YM, Scott GB, Morgan RS, Prestwich R, Bowles PA, Blair GE, Tanaka T, Rabbitts TH, Meade JL and Cook GP. Blocking oncogenic RAS enhances tumour cell surface MHC class I expression but does not alter susceptibility to cytotoxic lymphocytes. Mol Immunol 2014; 58: 160-168.

[36] Cheng H, Fan K, Luo G, Fan Z, Yang C, Huang Q, Jin K, Xu J, Yu X and Liu C. KrasG12D mutation contributes to regulatory T cell conversion through activation of the MEK/ERK pathway in pancreatic cancer. Cancer Lett 2019; 446: 103-111.

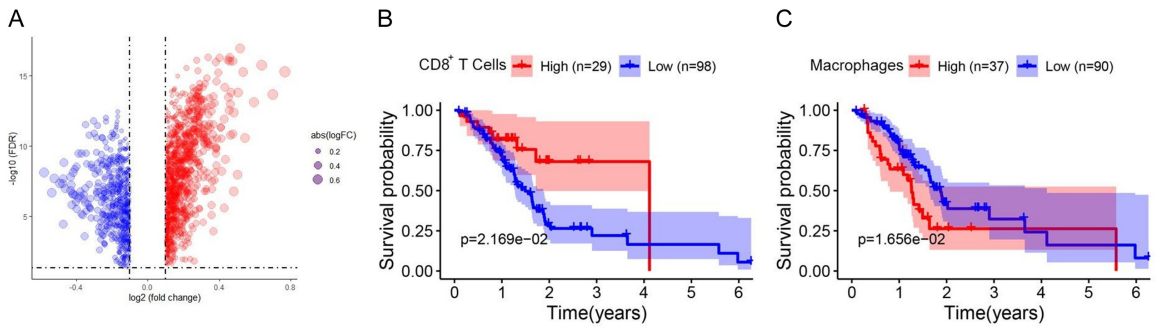

Figure S1. A. Identification of GEGs in PC. Volcano plot of genome-wide gene expression profiles in normal and tumor samples from the meta-GEO PC cohort. B. KM survival analysis showed that patients with lower infiltration levels of $CD8^+$ T cells had a short OS than those with higher infiltration levels of $CD8^+$ T cells ($P<0.05$). C. KM survival analysis showed that patients with higher infiltration of macrophages had a shorter OS ($P<0.05$) than those with lower infiltration of TAMs ($P<0.05$).

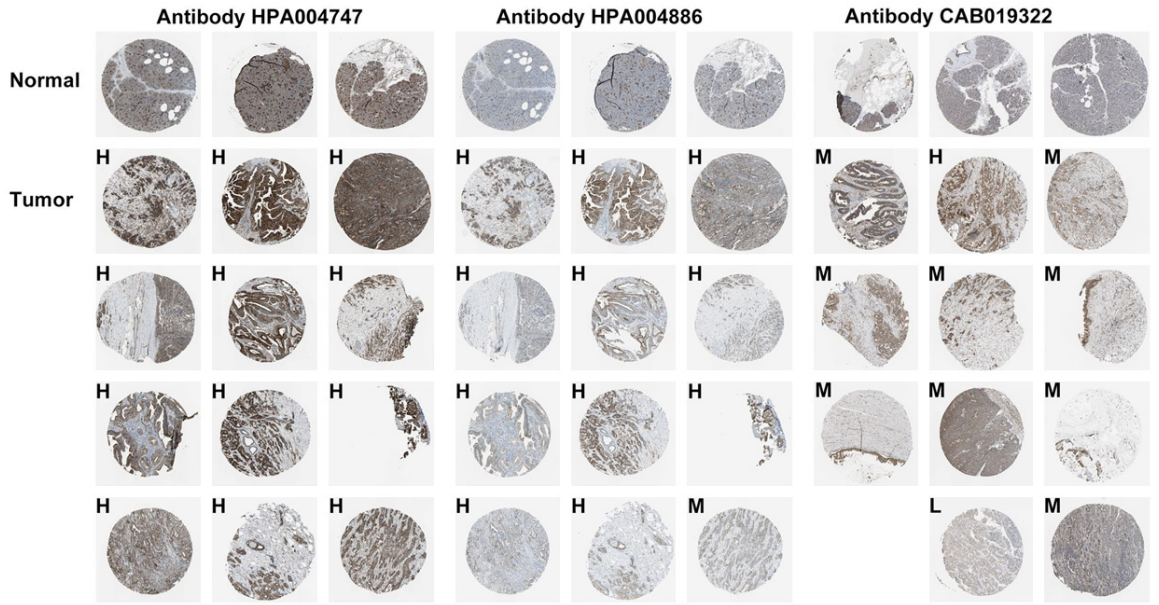

Figure S2. The Human protein Atlas database was used to validate the protein expression of FLNB, which demonstrated that the expression of FLNB was significantly upregulated in tumor tissues.

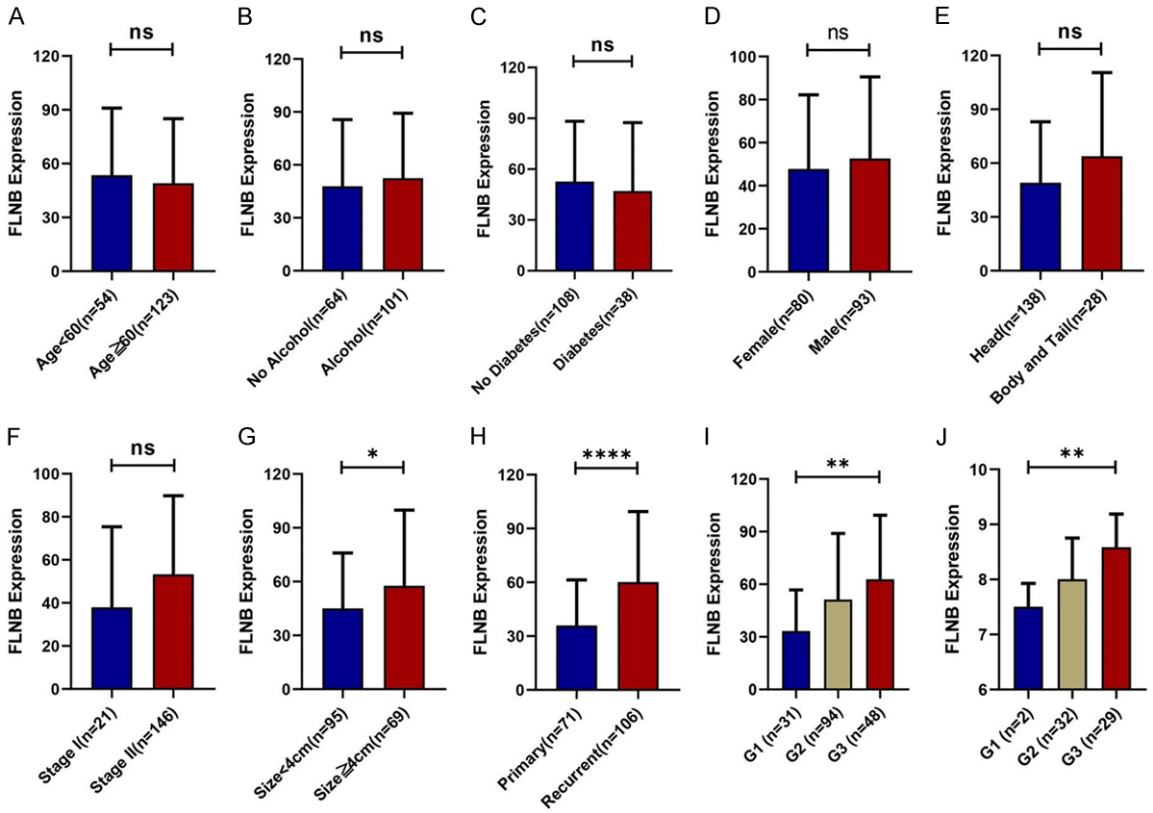

Figure S3. Association between FLNB expression and the clinicopathological features of PC. A-F. FLNB expression was not statistically associated with age, alcohol consumption history, diabetes status, gender, tumor site, and the AJCC stage. G, H. FLNB expression was positively associated with tumor size (*p*-value <0.05) andrecurrence (*p*-value <0.0001). I, J. FLNB expression in PC samples with higher histologic grade was obviously higher than that in PC samples with lower histologic grade (*p*-value <0.01) in both the TCGA and GSE62452 cohorts (*P<0.05; **P<0.01; ***P<0.001; ****P<0.0001).

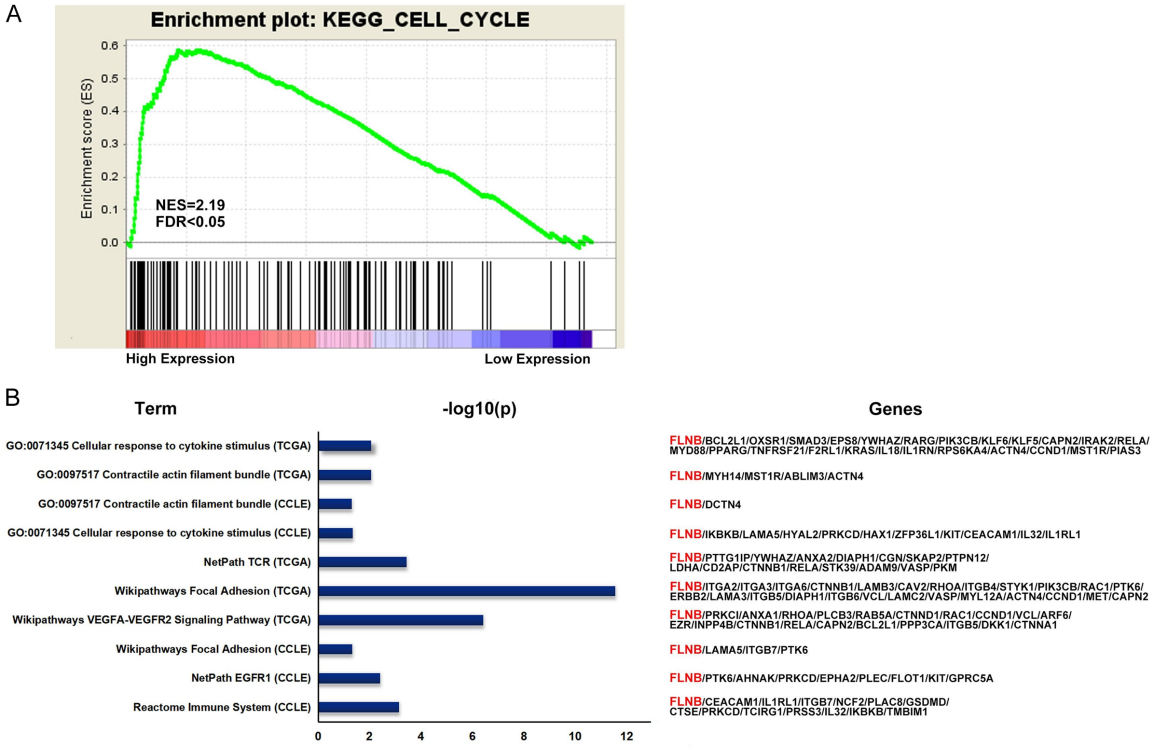

Figure S4. Functional enrichment analysis for FLNB. A. GSEA revealed that the cell cycle related gene set (NES=2.19, FDR<0.05) was enriched in the high-Exp group. B. GO enrichment analysis revealed that FLNB may play an important role in cellular response to cytokine stimulus and contractile actin filament bundle. Pathway enrichment analysis showed that FLNB may be involved in vascular formation (e.g. VEGFA-VEGFR2 signaling pathway or EGFR1), focal adhesion, and immune regulation (e.g. TCR).

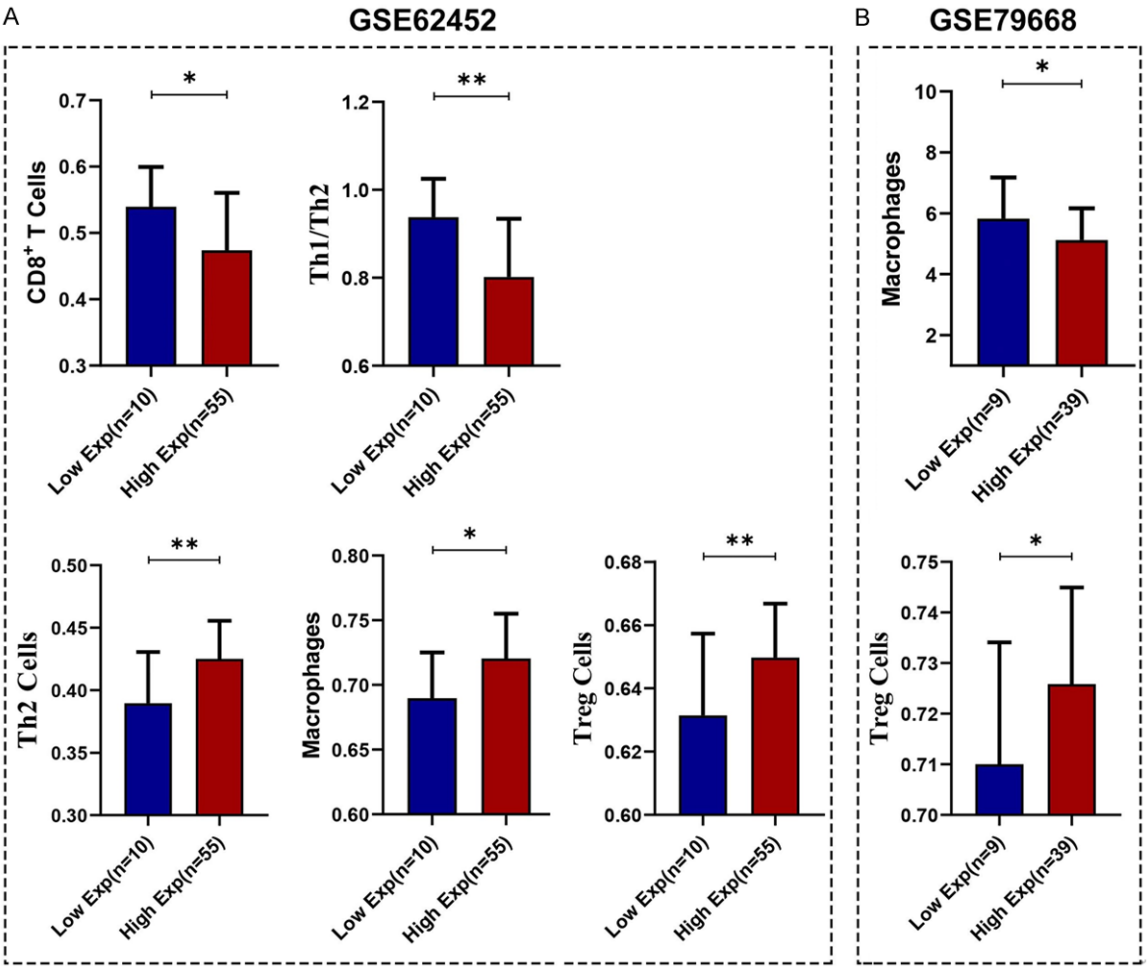

Figure S5. ssGSEA algorithm to validate the association between FLNB expression and immune infiltration within the tumor in the GSE62452 and GSE79668 cohorts. A. In the GSE62452 cohort, $CD8^+$ T cells and Th1/Th2 were significantly enriched in the low-Exp group, while Th2 cells, TAMs, and Treg cells were enriched in the high-Exp group. B. In the GSE79668 cohort, TAMs and Treg cells were enriched in the high-Exp group (*P<0.05; **P<0.01; ***P<0.001; ****P<0.0001).